INDEX COPERNICUS
INTERNATIONAL

Bio-Algorithms and Med-Systems

WWW.BAMSJOURNAL.COM ISSN: 1896-530X

ORIGINAL ARTICLE

Received: 27.11.2023
Accepted: 07.12.2023
Published: 31.12.2023

CITE THIS ARTICLE AS:
Das M, Mryka W, Beyene EY, Parzych S, Sharma S, Stepien E, Moskal P, on behalf of J-PET collaboration, "Estimating the efficiency and purity for detecting annihilation and prompt photons for positronium imaging with J-PET using toy Monte Carlo simulation," Bio-Algorithms and Med-Systems vol. 1, no. 1, pp. 87-95, 2023, DOI: 10.5604/01.3001.0054.1938

AUTHORS' CONTRIBUTION:
A – Study Design
B – Data Collection
C – Statistical Analysis
D – Data Interpretation
E – Manuscript Preparation
F – Literature Search
G – Funds Collection

CORRESPONDING AUTHOR:
Manish Das; Faculty of Physics, Astronomy and Applied Computer Science, Jagiellonian University, Krakow, Poland; S. Łojasiewicza street 11, 30-348 Krakow, Poland; E-mail: manishdasind@gmail.com

COPYRIGHT:
Some right reserved: Publishing House by Index Copernicus Sp. z o. o.

OPEN ACCESS:
The content of the journal „Bio-Algorithms and Med-Systems" is circulated on the basis of the Open Access which means free and limitless access to scientific data.

CREATIVE COMMONS CC, BY 4.0:
Attribution. It is free to copy, distribute, present and perform the copyrighted work and derivative works developed from

Estimating the efficiency and purity for detecting annihilation and prompt photons for positronium imaging with J-PET using toy Monte Carlo simulation

Manish Das[1,2ABCDEF] (ORCID: 0009-0001-2901-1745), Wiktor Mryka[1,2DE] (ORCID: 0009-0006-7616-8290), Ermias Y. Beyene[1,2E] (ORCID: 0009-0002-8757-2169), Szymon Parzych[1,2E], Sushil Sharma[1,2DE] (ORCID: 0000-0001-8947-0110), Ewa Stępień[1,2DEG] (ORCID: 0000-0003-3589-1715), Pawel Moskal[1,2ADEFG] (ORCID: 0000-0002-4229-3548), on behalf of J-PET collaboration

[1]Faculty of Physics, Astronomy and Applied Computer Science, Jagiellonian University, Krakow, Poland
[2]Centre for Theranostics, Jagiellonian University, Krakow, Poland

ABSTRACT

The positronium imaging technique represents a potential enhancement of the PET imaging method. Its core principle involves employing a β^+ radiation source that emits additional gamma (γ) quanta referred to as prompt gamma. Our aim is to evaluate the capability to differentiate between annihilation and prompt gamma emissions, a vital aspect of positronium imaging. For this purpose, the selected isotopes should enable high efficiency and purity in detecting both prompt gamma and annihilation gamma. The assessment of the efficiency in identifying prompt and annihilation photons for various isotopes, which are potentially superior candidates for $\beta^+ + \gamma$ emitters, is conducted through toy Monte-Carlo simulation utilizing the cross-section formula for photon-electron scattering. In this article, we have performed calculations for efficiency and purity values across different isotopes under ideal conditions and examined how these values evolve as we incorporate the fractional energy resolution into the analysis. Ultimately, the primary goal is to determine the energy threshold that optimizes both efficiency and purity, striking a balance between accurately identifying and recording events of interest while minimizing contamination from undesired events.

KEYWORDS

J-PET, Positronium imaging, PET, Medical imaging

INTRODUCTION

Positron Emission Tomography, commonly known as PET scanning, is a well-recognized and widely used medical diagnostic imaging technique [1, 2]. A novel technique referred to as positronium imaging was recently introduced within the field of Positron Emission Tomography (PET) [3–6]. Recently reported the first ex-vivo positronium images [7] inspire the development of methods for the registration of three photons from $\beta^+ + \gamma$ radionuclides.

The positronium imaging technique represents a potential enhancement of the PET imaging method [8, 9], and its core principle involves employing a β^+ radiation source that emits additional gamma (γ) quanta referred to as prompt gamma [10]. This technique in PET imaging represents an innovative approach that offers potential advantages over classical PET. It may offer improved spatial resolution and the potential for reduced radiation exposure to patients [11].

A notable advancement in multi-tracer PET techniques involves the adoption of dual-tracer imaging [12–15]. In this approach, one tracer employs a radioisotope that emits pure positrons (β^+), while the other utilizes a radioisotope that also emits high-energy prompt gamma ($\beta^+ + \gamma$). This dual-tracer method could enable the simultaneous investigation of two distinct biological processes [16, 17]. Tab. I. provides a list of isotopes with pure β^+emitters and those with both $\beta^+ + \gamma$ emissions.

Tab. I. The table presents a variety of β. emitters suitable for dual tracer imaging, as well as $\beta^+ + \gamma$ emitters and isotopes suitable for proton beam therapy, online monitoring, and calibration purposes. It's worth noting that the online monitoring source and calibration source also fall within the category of $\beta^+ + \gamma$ emitters.

β EMITTERS	^{18}F, ^{11}C, ^{13}N, ^{15}O
β⁺+ γ EMITTERS	^{68}Ga, ^{44}Sc, ^{22}Na, ^{55}Co, ^{72}As, ^{60}Cu, ^{14}O, ^{10}C, ^{52m}Mn, ^{110m}In, ^{82}Rb
ONLINE MONITORING	^{14}O, ^{10}C
CALIBRATION SOURCE	^{22}Na

Recently utilizing the $\beta^+ + \gamma$ technique with the J- PET scanner prototype constructed from 192 BC-420 plastic scintillator strips (measuring 7 × 19 × 300 mm^3) [18, 19] equipped with the triggerless data acquisition system [20] and using the ^{22}Na isotope, the first positronium image was obtained. The findings from this experiment revealed significant differences in positronium lifetime between healthy and cancerous tissues [7, 9]. During the PET scan the annihilation process of positron-electron pairs can occur in two ways: either directly, resulting in the production of photons, or through the creation of an intermediate positron-electron bound state known as positronium, which occurs in tissue about 40% of the time [21, 22].

In a recent study, the Positron Annihilation Lifetime Spectroscopy (PALS) was employed to assess positronium lifetime in diverse tissue samples, encompassing both healthy and diseased specimens, which revealed a noteworthy differentiation between the two categories [8, 9, 23]. Furthermore, innovative methods have recently been introduced for the meticulous examination and decomposition of positron annihilation lifetime spectra [24, 25].

Moreover, the introduction of novel positronium image reconstruction techniques utilizing maximum likelihood image estimation has yielded an improved spatial image resolution reaching 4 mm [26, 27]. The J-PET tomography has a trigger--less data acquisition system [20], which enables it to make multi--photon detection and this flexibility extends to the identification and registration of events involving double, triple, and even more coincident photons, which renders it suitable for positronium imaging, setting it apart from conventional PET.

In positronium imaging, it's crucial to highlight that the isotopes should exhibit a minimal delay time, typically within the range of a few picoseconds. Delay time denotes the average time difference between the emission of positron and the emission of prompt gamma. A short delay time is essential because it provides critical information about the timing of positron emission, enabling the prompt gamma emission time, to serve as the starting time for determining positronium lifetime. In addition to this, the positron range plays a crucial role. A shorter positron range is preferable since in the calculation of the time of emission of prompt gamma it is assumed that annihilation and positron formation were at the same position. In order to calculate the prompt gamma emission time, its time of interaction in the detector is corrected for the time of flight between the emission point and interaction place in the detector. In addition to that, to maximize the likelihood of signal detection for the positronium imaging, it should have a high $\beta^+ + \gamma$ branching ratio ($Y_{\beta^+ + \gamma}$), along with a high β^+ branching (Y_{β^+}). $Y_{\beta^+ + \gamma}$ represents the fraction of the prompt gammas associated with the β^+ decay.

Tab. II. presents a comprehensive list of the discussed parameters and physical properties of the radionuclides that have the potential to be considered as suitable candidates [11, 33] for the positronium imaging technique. In the subsequent section, we will explore various properties and criteria, elaborating on the earlier discussion, which are considered essential for isotopes to be regarded as suitable candidates for this technique. However, it's worth noting that not all isotopes necessarily adhere to all of these criteria.

Within the realm of positronium imaging, the critical objective lies in the effective differentiation of the annihilation signal from the prompt gamma signal, as this is essential for achieving precise measurements of positronium lifetime. This article primarily centers on examining the efficiency and purity of distinguishing prompt photons from annihilation photons. The calculations are performed by employing the cross-section formula for Compton photon--electron scattering.

Tab. II. The table incorporates information on the half-life ($T_{1/2}$), the branching ratio of the positrons ($Y_{\beta+}$), the maximum positron energy (E_{MAX}), the mean range of positron in water (R_{MEAN}) [28], the calculated values of the mean range are consistent within 10% with the results obtained in reference [29], the energy of the prompt gamma (E_γ), the branching ratio of the prompt gamma (E_γ), the branching ratio of the pure $\beta^+ + \gamma$ events removing the electron capture contribution ($Y_{\beta^+ + \gamma}$) (subject to large errors) [30], the mean time interval between the emission of positron and prompt gamma (delay) and the maximum energy of electron achievable in the Compton scattering of the prompt gamma with the electron (Comp. E.) for selected isotopes for positronium technique [11, 31–33].

ISOTOPE	$T_{1/2}$	$Y_{\beta+}$ (%)	E_{MAX} (MeV)	R_{MEAN} (MM)	E_γ (MeV)	Y_γ(%)	$Y_{\beta+\gamma}$ (%)	$Y_{\beta+\gamma}/Y_{\beta+}$	DELAY (ps)	COMP. E. (MeV)
^{22}Na	2.60 y	89.95	0.545	0.54	1.275	99.94	89.90	99.94	3.6	1.062
^{44}Sc	3.97 h	94.3	1.474	1.69	1.157	99.9	94.3	100	2.61	0.948
^{68}Ga	67.71 m	88.91	1.899	2.25	1.077	3.22	1.19	1.34	1.57	0.870
^{60}Cu	23.7 m	92.59	0.653	0.67	1.333	88	81	87.48	0.735	1.118
					1.791	45.4	42	45.36	–	1.567
					0.826	21.7	20.4	22.03	0.59	0.631
^{72}As	26.0 h	87.86	3.33	4.27	0.834	81	71	80.81	3.35	0.638
^{82}Rb	1.26 m	95.36	3.382	4.34	0.777	15.1	13.5	14.16	4.45	0.584
^{55}Co	17.53 h	75.89	1.5	1.72	0.931	75	59	77.74	8	0.731
					0.477	20.2	13.5	17.79	37.9	0.311
					1.409	16.9	11.3	14.89	37.9	1.192
^{124}I	4.17 d	22.69	1.822	2.15	0.603	62.9	12	52.89	6.2	0.423
					0.723	10.36	0.25	4.58	1.04	0.534
^{10}C	19.3 s	99.97	2.93	3.69	0.718	100	99.97	100	710	0.530
^{14}O	70.6 s	99.89	1.808	2.13	2.313	99.39	99.26	99.38	0.068	2.083

Additionally, it aims to determine the optimal energy threshold required to maximize efficiency and purity for both annihilation and prompt gamma signals. For this purpose, a single threshold is defined for the deposited energy, prompt photons are then distinguished based on the deposited energy greater than the threshold (indicating they are above the threshold) and annihilation photons are less than the threshold (indicating they are below the threshold) as described in Fig. 5.

The efficiency of the annihilation or prompt gamma, in this context, refers to the measure of how effectively a simulation or measurement system captures and correctly identifies annihilation and prompt gamma rays. It is calculated as the ratio of the number of annihilation/prompt gamma rays correctly identified by the system to the total number of annihilation/prompt gamma rays. On the other hand, purity is a measure of the system's accuracy in correctly identifying annihilation and prompt gamma rays while minimizing the inclusion of other types of gamma rays. Efficiency and purity studies become even more critical when dealing with different isotopes in medical imaging as each isotope has unique emission characteristics and energy levels.

Understanding the efficiency and purity of specific isotopes is crucial for optimizing imaging techniques, ensuring that diagnostic tools can effectively capture and identify relevant anatomical or pathological features within the body.

Prior research has already explored similar studies involving only four potentially suitable candidates for positronium imaging, focusing on those isotopes that emit a single prompt gamma. These investigations were conducted utilizing simulation software such as GATE and J-POS [34].

This article primarily relies on the utilization of toy Monte Carlo simulations to gain insights into various parameters at a simulation level.

PROPERTIES OF $\beta^+ + \gamma$ EMITTERS

There are several criteria that the isotopes should fulfill in order to become a potentially useful candidate for the positronium imaging technique. The following criteria as discussed in the references [11, 33]:

- To obtain a precise estimation of the positronium lifetime, it is essential for the prompt gamma rays to be emitted shortly (delay), typically within a few picoseconds, following the β^+decay. Furthermore, these prompt gamma rays should have higher energy than annihilation photons.

- The positron mean range should be as low as possible, as it aids in accurately determining the moment of positronium

formation, enabling a more precise measurement of positronium lifetime. Additionally, a reduced mean positron range contributes to enhanced spatial resolution [35, 36].

- To maximize the likelihood of signal detection for the positronium imaging, it is essential that both the β^+ branching ratio and the $\beta^+ + \gamma$ branching ratio should be as high as possible.
- The radionuclide's half-life should be well-suited for clinical applications.
- To achieve enhanced image quality with minimized noise, the radioisotope of interest should emit only a few additional γ lines (preferably one).
- The radioisotope should possess a viable production pathway as discussed for different isotopes in reference [11].
- Finally, the efficiency and purity for the annihilation and prompt gamma should be as high as possible for a defined threshold, a matter that will be examined in this article.

It's important to acknowledge that not all isotopes necessarily meet all these criteria, but there are some isotopes that come close to fulfilling them. In this article, we introduce the most promising radioisotopes. Comprehensive details regarding the physical properties of these candidates are available in Tab. II. The decay schemes for all the isotopes under examination in this article are illustrated in Fig. 1.

METHOD

As previously discussed, the evaluation of the efficiency and purity in identifying prompt and annihilation photons among the different $\beta^+ + \gamma$ emitters is performed using a toy Monte Carlo simulation. This simulation incorporates the cross-section formula for Compton photon-electron scattering.

The cross-section formula for the scattered electron due to Compton scattering is given by Klein and Nishina, which gives the probability of imparting an energy ΔE to the electron [37]. It can be calculated from the Klein-Nishina equation given by

$$\frac{d\sigma}{d\Delta E} = \frac{r_0^2 mc^2}{(E_0 - \Delta E)^2}\left\{\left[\frac{mc^2 \Delta E E_0^2}{E_0^2}\right] + 2\left[\frac{E_0 - \Delta E}{E_0}\right]^2 + \frac{E_0 - \Delta E}{E_0^3}[(\Delta E - mc^2)^2 - (mc^2)^2]\right\}. \quad (1)$$

In Equation (1) the following notations was used:

$d\sigma/d\Delta E$ = Energy distribution of the scattered electron, r_0 = The classical electron radius, m = Electron rest-mass, c = Velocity of electromagnetic radiation in a vacuum, ΔE = Kinetic energy of the recoiled electron/energy loss of the photon, E_0 = Initial photon energy. The maximum value of the cross-section occurs at ΔE_{max}, representing the maximum energy attainable by an electron, commonly referred to as the Compton edge [37]:

$$\Delta E_{max} = E_0\left[1 - \frac{1}{1 + 2\frac{E_0}{mc^2}}\right]. \quad (2)$$

Through Monte-Carlo simulation and utilizing the Klein-Nishina equation, events are generated for electrons scattered by annihilation and prompt photons for each isotope. Fig. 2. displays the electron energy distributions for annihilation and prompt gamma emissions for different isotopes.

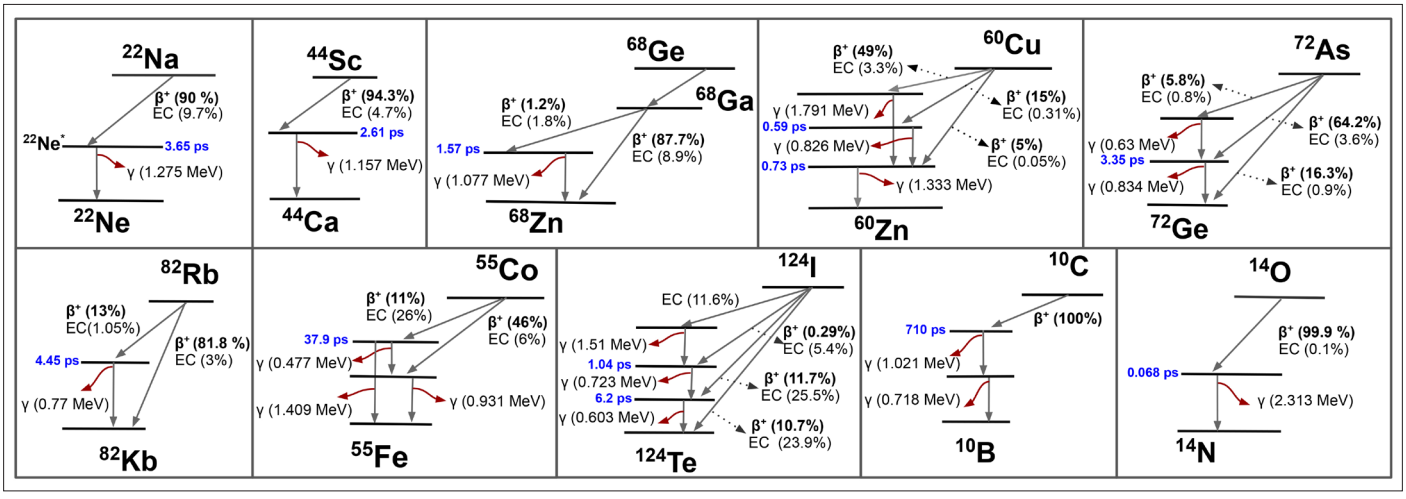

Fig. 1. The decay schemes for the isotopes ^{22}Na, ^{44}Sc, ^{68}Ga, ^{60}Cu, ^{72}As, ^{82}Rb, ^{55}Co, ^{124}I, ^{10}C, and ^{14}O are presented in the same order as they appear in the Tab. II. These decay schemes exclusively highlight the β^+ decays followed by the emission of a prompt gamma [30]. It's important to note that the total β^+ branching ratio may vary between the decay schemes and the table due to this selective representation. In the decay schemes, β^+ (" ") denotes the β^+ branching, EC (" ") indicates Electron Capture contributions, and γ (" ") represents the energy of the prompt gamma. Additionally, the delay time is presented in blue text for clarity. The delay time denotes the average time between the emission of positron and the emission of prompt gamma.

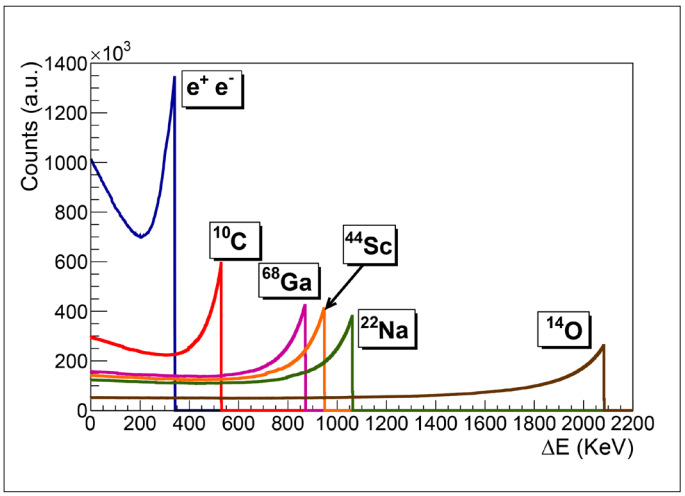

Fig. 2. Simulated energy loss spectra for annihilation (0.511 MeV) and de--excitation photons for various isotopes, particularly those emitting a single prompt gamma.

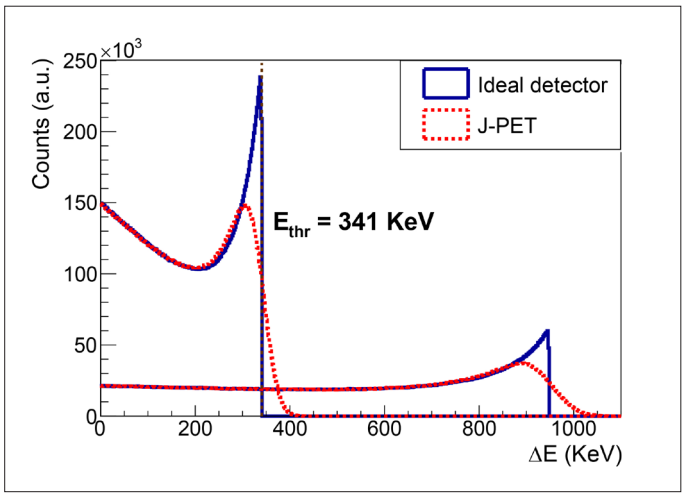

Fig. 3. Effect of the energy resolution of the J-PET detector in the simulated energy loss spectra for annihilation (0.511 MeV) and de-excitation photons emitted from the ^{44}Sc radionuclide.

The fractional energy resolution for energy deposition (ΔE) by gamma quanta through Compton scattering in the J-PET scanner prototype constructed from 192 BC-420 plastic scintillator strips (measuring 7 × 19 × 300 mm^3), is reported to be [18]:

$$\frac{\sigma(\Delta E)}{\Delta E} = \frac{0.044}{\sqrt{\Delta E(MeV)}}\,. \tag{3}$$

When we incorporate the fractional energy resolution of the detector (as defined in Equation 3) into our simulation, the influence of the detector's response becomes evident, as depicted in Fig. 3.

Due to the smearing caused in the energy resolution, even when a threshold is set at 341 keV, certain events from the annihilation region may still be detected within the prompt photon region. This overlap produces impurity in the analysis.

It's important to emphasize that this toy Monte Carlo simulation involves a pure signal, meaning there are no background signals to consider. Additionally, since no detector geometry is involved, all events are generated solely based on the probability density function and are assumed to be detected. For the ideal case as defined in Fig. 4., and when considering the incorporation of fractional energy resolution, as depicted in Fig. 5., various parameters can be defined as follows:

$$\epsilon_a = \frac{N_a(\Delta E < 341keV)}{N_a} \tag{4}$$

$$P_a = \frac{N_a(\Delta E < 341keV)}{N_a(\Delta E < 341keV) + N_p(\Delta E < 341keV)} \tag{5}$$

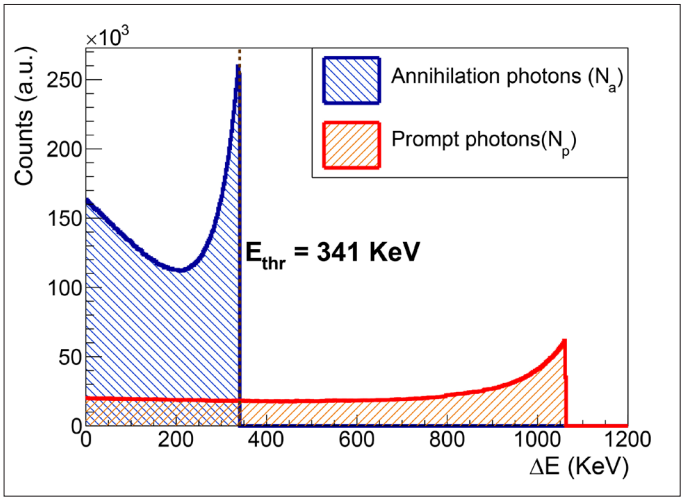

Fig. 4. Simulated energy loss spectra for annihilation (0.511 MeV) and de-excitation photons emitted from the ^{22}Na radionuclide. The results were obtained for the ideal detector.

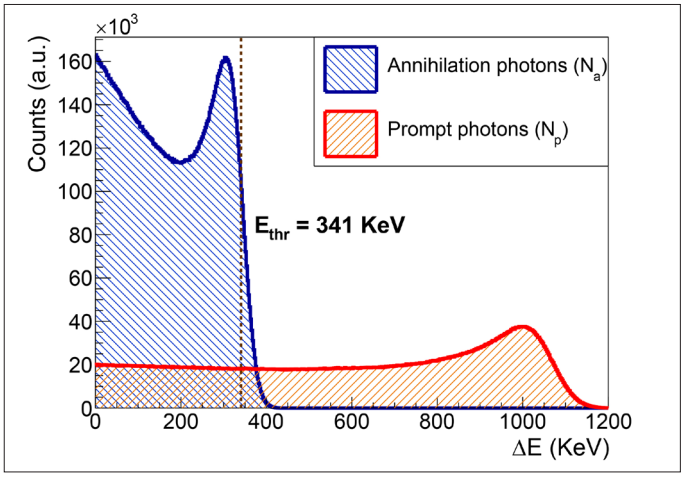

Fig. 5. Simulated energy loss spectra for annihilation (0.511 MeV) and de--excitation photons emitted from the ^{22}Na radionuclide. The results were obtained by taking experimental energy resolution of the J--PET detector into account.

$$\epsilon_p = \frac{N_p(\Delta E > 341keV)}{N_p} \quad (6)$$

$$P_p = \frac{N_p(\Delta E > 341keV)}{N_p(\Delta E > 341keV) + N_a(\Delta E > 341keV)}. \quad (7)$$

where $\in_a$ denotes the efficiency of identifying the annihilation photon, P_a denotes purity of selecting the annihilation photon, $\in_p$ denotes efficiency of identifying the prompt gamma and, P_p denotes purity of selecting the prompt gamma.

In the ideal scenario where smearing is absent, identifying annihilation gamma rays achieves a perfect efficiency rate of 100%. Moreover, the purity of the selection process for prompt gamma rays is likewise at its peak with a 100% purity level, as every event above the 341 keV threshold directly corresponds to a prompt gamma. However, after smearing of the energy loss spectra by the experimental resolution the values of the $\in_a$ and P_p will be smaller than 100%. The detailed results are presented in the result section.

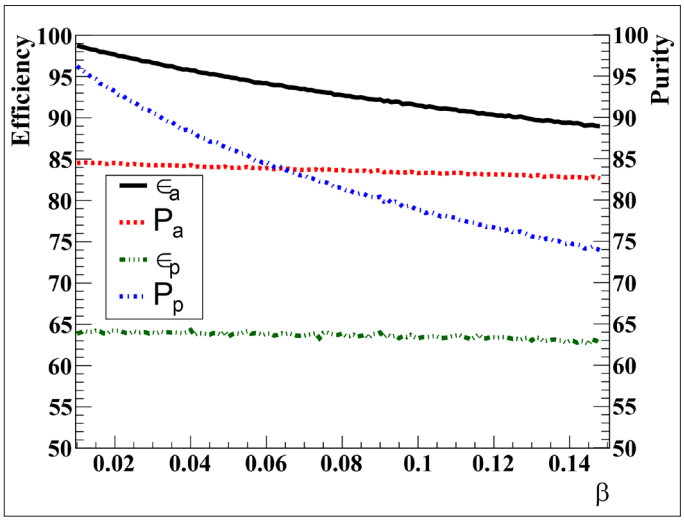

Fig. 6. Dependence of efficiency and purity for annihilation and prompt gamma on parameter for ^{44}Sc isotope with an energy threshold set at 341 keV, where β = 0.044 in the case of the J-PET detector. It is evident that the efficiency for annihilation gamma and the purity for prompt gamma both experience a notable decrease.

RESULT AND DISCUSSION

Initially, we investigated the influence of the fractional energy resolution of the J-PET detector on the efficiency and purity of annihilation and prompt gamma identification. This examination involves the calculation of the standard deviation using Equation 3.

$$\sigma(\Delta E) = \beta \times \sqrt{\Delta E(MeV)}. \quad (8)$$

where β = 0.044 in the J-PET single detection module built out from the BC-420 plastic scintillator strip [18]. If we vary the value of β, this will ultimately lead to changes in the fractional resolution of the detector. The correlation between β and various parameters can be observed in Fig. 6., where the value of β is varied from 0.01 to 0.15.

Furthermore, the value of the efficiency and purity for different isotopes mentioned earlier has been calculated via toy Monte-Carlo simulations, with an energy threshold set at 341 keV. The outcomes of these simulations are showcased in Tab. III. and Fig. 7.

In summarizing the results from the Tab. IV., we observe that for ^{14}O, there is excellent purity for both prompt and annihilation (511 keV) photons, with nearly 100% efficiency for annihilation photons. Unfortunately, its short half-life of 70.6 seconds renders it difficult for medical imaging.

^{60}Cu, ^{22}Na, and ^{44}Sc isotopes exhibit high efficiency and purity for both prompt and annihilation gamma radiation, making them suitable candidates for positronium imaging.

However, in the case of ^{60}Cu, it's important to note that it produces multiple prompt gammas, which may introduce noise to the imaging.

Tab. III. Table summarising the different values of efficiency and purity for annihilation and prompt gamma with an energy threshold set at 341 keV. The value of $\in_a$ for J-PET is not shown here since the efficiency of identifying the annihilation gamma ($\in_a$) is 95.41%, as it doesn't depend on the prompt gamma events.

ISOTOPES	E_γ (MeV)	IDEAL		J-PET		
		$\in_p$(%)	P_a (%)	P_a (%)	$\in_p$(%)	P_p (%)
^{22}Na	1.275	87.97	72.93	85.72	68.20	88.12
^{44}Sc	1.157	86.59	69.03	84.14	64.04	87.42
^{68}Ga	1.077	99.77	66.29	99.72	60.97	8.17
^{60}Cu	1.333	89.9	74.31	87.68	69.35	86.93
	1.791	96.30	83.08	95.55	80.39	79.97
	0.826	94.94	51.60	94.11	45.78	52.35
^{72}As	0.834	83.78	52.08	81.49	46.38	80.35
^{82g}Rb	0.777	96.43	47.78	95.85	41.59	39.22
^{55}Co	0.931	86.09	58.43	84.04	53.37	81.95
	0.477	91.83	0	91.50	0.35	0.69
	1.409	98.24	76.00	97.82	71.52	53.59
^{124}I	0.603	83.65	26.08	81.73	19.37	52.67
	0.723	99.68	42.48	99.62	35.6	4.11
^{10}C	0.718	77.63	42.35	74.77	35.59	79.51
^{14}O	2.313	94.45	88.17	93.86	87.42	90.42

^{22}Na, with its very long half-life of 2.6 years, is not well-suited for medical imaging applications; however, it finds utility in various fundamental physics experiments [38].

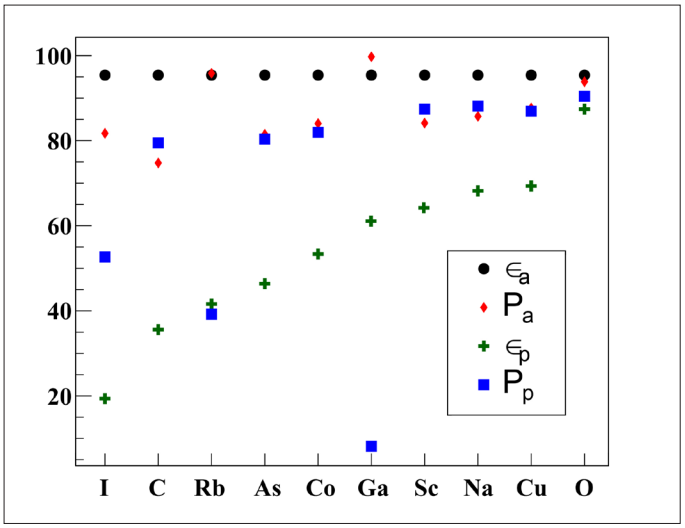

Fig. 7. Efficiency and purity measurements for different isotopes with an energy threshold set at 341 keV. For isotopes that produce multiple prompt gammas, only the primary gamma line with a high $\beta^+ + \gamma$ yield is included here. The isotopes in the figure are organized in ascending order of the prompt gamma efficiency.

Tab. IV. Table summarising the values for optimized threshold (T_{OPT}) and corresponding efficiency and purity for annihilation and prompt gamma for different isotopes.

ISOTOPES	E_γ (MeV)	T_{OPT} (keV)	$\in_a$(%)	P_a (%)	$\in_p$(%)	P_p (%)
^{22}Na	1.275	373	99.42	85.07	65.09	98.25
^{44}Sc	1.157	375	99.51	83.38	60.34	98.41
^{68}Ga	1.077	418	99.99	99.68	52.09	98.69
^{60}Cu	1.333	376	99.54	87.30	66.9	98.46
	1.791	390	99.88	95.06	77.14	99.32
	0.826	383	99.76	93.72	39.32	94.77
^{72}As	0.834	367	99.07	80.92	42.20	94.81
^{82g}Rb	0.777	387	99.83	95.51	33.78	93.54
^{55}Co	0.931	375	99.49	83.33	48.80	97.43
	0.477	125	37.71	91.33	59.76	7.86
	1.409	395	99.93	97.61	67.14	98.6
^{124}I	0.603	360	98.49	81.40	14.9	72.29
	0.723	409	99.99	99.58	24.04	90.92
^{10}C	0.718	357	98.15	74.36	32.34	89.71
^{14}O	2.313	389	99.86	93.14	85.19	99.68

Among these candidates, ^{44}Sc stands out as one of the most promising radioisotopes for $\beta^+ + \gamma$ imaging [39]. It is the best choice for establishing the proof of concept for the positronium imaging technique. ^{44}Sc isotope has a convenient half-life and emits only one high intensity prompt γ with an energy of 1157 keV.

In the case of ^{68}Ga isotope, it's evident that the purity of the prompt gamma is low due to the very small probability of prompt photon emission (1.19%), which makes it unsuitable for $\beta^+ + \gamma$ tomography applications. The result also indicates that when using ^{68}Ga a higher threshold should be used. For example, when applying the threshold of 418 keV the purity for the prompt gamma increases to 98.69%.

^{55}Co isotope can also be considered for positronium imaging technique, as it emits a single high-intensity γ line [40]. However, it's important to note that this isotope emits two additional low-intensity γ lines, that makes the analysis more complicated.

Furthermore, there are various other isotopes such as ^{72}As, ^{82g}Rb, ^{10}C, ^{124}I, which can be also useful for the positronium imaging [11].

The results clearly demonstrate that the isotopes have different values of efficiency and purity if the energy threshold is set at 341 keV. When the threshold value is increased, the efficiency and purity for both annihilation and prompt gamma undergo changes, as it is evident in Fig. 8.

To find the optimum energy threshold that achieves the equilibrium between enhancing the efficiency of identifying the events of interest and maintaining purity by reducing the impact of unwanted events and contamination, we define a term referred to as "figure of merit" (FoM), which can be defined in terms of efficiency and purity as follows:

$$FoM = \in_\alpha \times \in_p \times P_\alpha \times P_p. \quad (9)$$

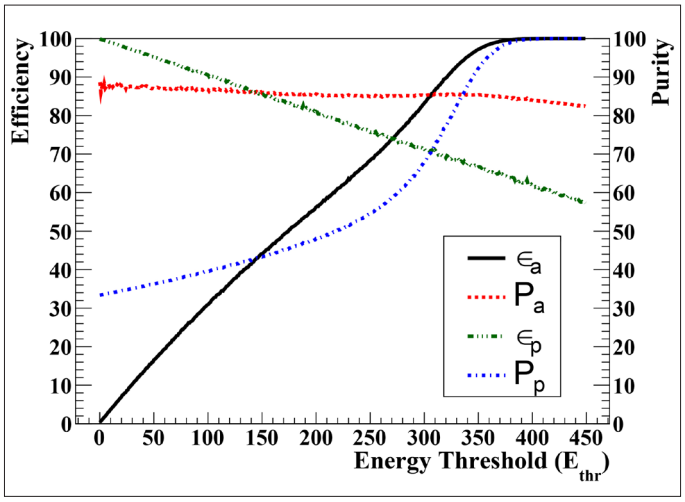

Fig. 8. Dependence of the efficiency and purity on energy threshold for identification of annihilation photons and prompt gamma emitted by the ^{22}Na isotope. All the events below the threshold would be treated as annihilation, whereas events above the threshold would be treated as prompt gamma.

Such defined FoM is a measure of the goodness of the event selection for the positronium imaging. As the optimum energy threshold, we choose the one for which FoM reaches its maximum

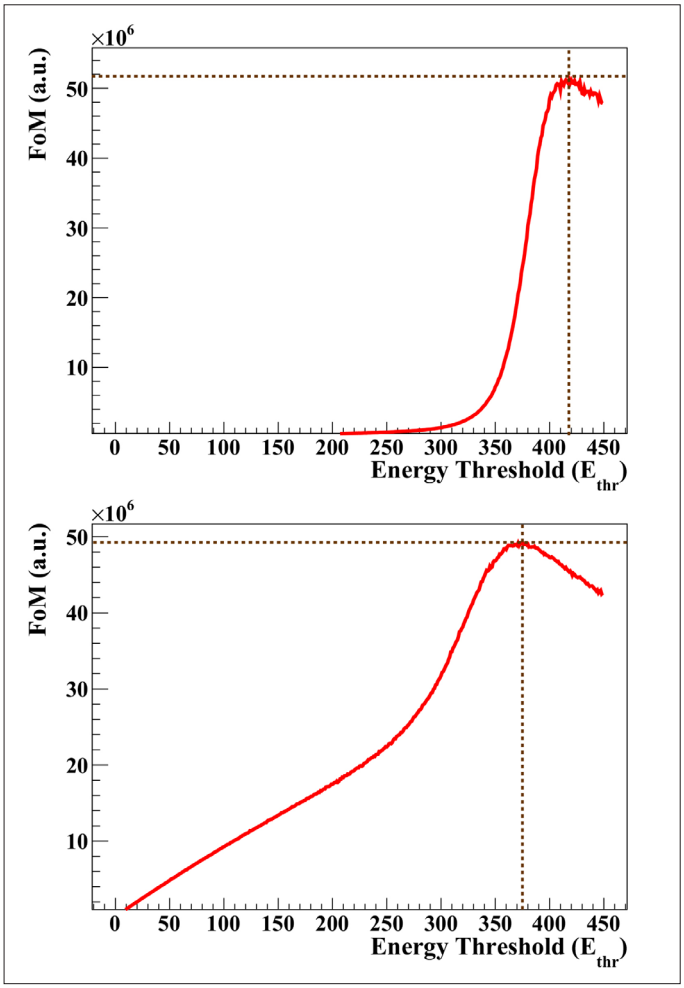

Fig. 9. A graphical representation depicts the relationship between the Figure of Merit and the threshold for ^{68}Ga (upper image) and ^{44}Sc (lower image) isotope. A horizontal dashed line indicates the peak value of FoM (measured in arbitrary units), and a vertical line signifies the optimum energy threshold.

value. Tab. IV. summarizes the optimal threshold values and corresponding efficiency and purity for various isotopes, while Fig. 9. presents a FoM *versus* energy threshold for ^{68}Ga and ^{44}Sc isotope.

CONCLUSION

Positronium imaging holds the potential to enhance PET imaging methodologies significantly [4, 10]. At its core, positronium imaging relies on the selection of isotopes that emit de-excitation gamma radiation. The key lies in distinguishing between annihilation and prompt gamma emissions. This paper provides a comprehensive summary of isotope properties suitable for positronium imaging, with a thorough analysis of the efficiency and purity of identification of annihilation photon and prompt gamma. Furthermore, we determine the optimal threshold to maximize efficiency and purity for different isotopes. Notably, ^{44}Sc could be the most promising candidate for the positronium imaging, also meeting criteria for medical imaging purposes. Our study employs a simplified toy Monte Carlo simulation, it offers valuable insights into potential future investigations exploring diverse isotopes for positronium imaging applications.

ACKNOWLEDGMENT

We acknowledge support from the Foundation for Polish Science through the TEAM POIR.04.04.00-00-4204/17 program, the National Science Centre of Poland through Grants No. 2021/42/A/ST2/00423, and No. 2021/43/B/ST2/02150, Jagiellonian University via Project No. CRP/0641.221.2020, and the SciMat and qLife Priority Research Area budget under the auspices of the program Excellence Initiative – Research University at Jagiellonian University.

REFERENCES

1. Alavi A, Werner TJ, Stępień EŁ, Moskal P. Unparalleled and revolutionary impact of PET imaging on research and day to day practice of medicine. Bio-Algorithms and Med-Systems 2021;17:203-12.
2. Vandenberghe S, Moskal P, Karp JS. State of the art in total body PET. EJNMMI Phys. 2020;7:1-33.
3. Moskal P, Positronium Imaging, 2019 IEEE Nuclear Science Symposium and Medical Imaging Conference (NSS/MIC), Manchester, UK, 2019; pp. 1-3. https://ieeexplore.ieee.org/document/9059856.
4. Moskal P, Stępień E. Perspectives on translation of positronium imaging into clinics. Front. Phys. 2022;10: 969806.
5. Moskal P, Kisielewska D, Curceanu C, Czerwiński E, Dulski K, Gajos A, et al. Feasibility study of the positronium imaging with the J-PET tomograph. Phys. Med. Biol. 2019;64:055017.
6. Moskal P, Kisielewska D, Y. Shopa R, Bura Z, Chhokar J, Curceanu C, et al. Performance assessment of the 2 γpositronium imaging with the total-body pet scanners. EJNMMI Phys. 2020;7(1):44.
7. Moskal P, Dulski K, Chug N, Curceanu C, Czerwiński E, Dadgar M, et al. Positronium imaging with the novel Multiphoton Pet Scanner. Sci. Adv. 2021;7(42):eabh4394.
8. Karimi H, Moskal P, Żak A, Stępień E. 3D melanoma spheroid model for the development of positronium biomarkers. Sci Rep. 2023;13:7648.
9. Moskal P, Kubicz E, Grudzień G, Czerwiński E, Dulski K, Leszczyński B, et al. Developing a novel positronium biomarker for Cardiac Myxoma Imaging. EJNMMI Phys. 2023;10(1):22.
10. Moskal P, Stępień EŁ. Prospects and Clinical Perspectives of Total-Body PET Imaging Using Plastic Scintillators. PET Clinics 2020;15:439-52.
11. Sitarz M, Jean-Pierre Cussonneau, Matulewicz T, Haddad F. Radionuclide candidates for β+γ coincidence PET: An overview. Appl Radiat Isot 2020;155:108898-8.
12. Uenomachi M, Shimazoe K, Takahashi H. A double photon coincidence detection method for medical gamma-ray imaging. Bio-Algorithms and Med-Systems 2022;18:120-6.
13. Fukuchi T, Shigeta M, Haba H, Mori D, T. Yokokita, Komori Y, et al. Image reconstruction method for dual-isotope positron emission tomography. J. Instrum. 2021;16:P01035-5.
14. Pratt EC, Lopez-Montes A, Volpe A, Crowley MJ, Carter LM, Mittal V, et al. Simultaneous quantitative imaging of two pet radiotracers via the

detection of positron–electron annihilation and prompt gamma emissions. Nat. Biomed. Eng. 2023;7(8):1028-39.

15. Beyene EY, Das M, Durak-Kozica M, Korcy G, Mryka W, Niedzwiecki S, et al. Exploration of simultaneous dual-isotope imaging with multi-photon modular J-PET scanner. Bio-Algorithms and Med-Systems. 2023;19:101-8.
16. Andreyev A, Celler A. Dual-isotope PET using positron-gamma emitters. Phys. Med. Biol. 2011;56:4539-56.
17. Kadrmas DJ, Hoffman JM. Methodology for Quantitative Rapid Multi--Tracer PET Tumor Characterizations. Theranostics 2013;3:757-73.
18. Moskal P, Niedźwiecki Sz, Bednarski T, Czerwiński E, Kapłon, Kubicz E, et al. Test of a single module of the J-PET scanner based on plastic scintillators. Nucl. Instrum. Methods Phys. Res. A: Accel. Spectrom. Detect. Assoc. Equip. 2014;764:317-21.
19. Niedźwiecki S, Białas P, Curceanu C, Czerwiński E, Dulski K, Gajos A, et al. J-pet: A new technology for the whole-body pet imaging. Acta Phys. Pol. B 2017;48(10):1567.
20. Korcyl G, Hiesmayr BC, Jasinska B, Kacprzak K, Kajetanowicz M, Kisielewska D, et al. Evaluation of single-chip, real-time tomographic data processing on FPGA SOC devices. IEEE Trans Med Imaging. 2018;37(11):2526-35.
21. Moskal P, Jasińska B, Stępień EŁ, Bass SD. Positronium in medicine and biology. Nat. Rev. Phys 2019;1:527-9.
22. Bass SD, Mariazzi S, Moskal P, Stępień E. Colloquium: Positronium physics and biomedical applications. RMP 2023;95:021002.
23. Jasińska B, Zgardzińska B, Chołubek G, Pietrow M, Gorgol M, Wiktor K, et al. Human tissue investigations using pals technique - free radicals influence. Acta Phys. Pol. 2017;132(5):1556-9.
24. Dulski K, on behalf of the J-PET collaboration on. PALS Avalanche - A New PAL Spectra Analysis Software. Acta Phys. Pol. 2020;137:167-70.
25. Shibuya K, Saito H, Tashima H, Yamaya T. Using inverse Laplace transform in positronium lifetime imaging. Phys. Med. Biol. 2022;67:025009.
26. Qi J, Huang B. Positronium Lifetime Image Reconstruction for TOF PET. IEEE Trans Med Imaging 2022;41(10):2848-55.
27. Huang H-H, Zhu Z, Booppasiri S, Chen Z, Pang S, Kao C-M. A statistical reconstruction algorithm for positronium lifetime imaging using time--of-flight positron emission tomography [Preprint]. 2023 [posted 2022 Jun 13; revised 2022 Jul 21; revised 2023 Mar 5; revised 2023 Nov 22; cited 2023 Dec 19]. Available from: https://arxiv.org/abs/2206.06463v4.
28. Mryka W, Manish Das M, Beyene EY, Moskal P, Stępień E, On behalf of J-PET collaboration. Estimating influence of positron range in proton therapy beam monitoring with PET. Bio-Algorithms and Med-Systems. 2023;19:96-100.
29. Kertész H, Beyer T, Panin V, Jentzen W, Cal-González J, Berger A, et al. Implementation of a Spatially-Variant and Tissue-Dependent Positron Range Correction for PET/CT Imaging. Front. Physiol. 2022;13:818463.
30. International Atomic Energy Agency (IAEA), livechart of nuclides [Internet]. Available from: https://www-nds.iaea.org/relnsd/vcharthtml/VChartHTML.html.
31. Conti M, Eriksson L. Physics of pure and non-pure positron emitters for PET: a review and a discussion. EJNMMI Phys 2016;3(1):8.
32. George KJH, Borjian S, Cross MC, Hicks JW, Schaffer P, Kovacs MS. Expanding the PET radioisotope universe utilizing solid targets on small medical cyclotrons. RSC Adv 2021;11:31098-123.
33. Matulewicz T, Radioactive nuclei for $\beta + \gamma$ PET and theranostics: selected candidates. Bio-Algorithms and Med-Systems 2021;17:235-9.
34. Masełek R, Krzemien W, Klimaszewski K, Raczyński L, Kowalski P, Shopa R, et al. Towards 2+1 photon tomography: Energy-based selection of two 511 kev photons and a prompt photon with the J-pet scanner [Internet]. 2018 [posted 2018 March 2; cited 2023 Dec 19]. Available from: https://doi.org/10.48550/arXiv.1803.00996.
35. Beekman FJ, Kamphuis C, Koustoulidou S, Ramakers RM, Goorden MC. Positron range-free and multi-isotope tomography of positron emitters. Phys. Med. Biol. 2021;66:065011-1.
36. Thirolf PG, Lång C, Parodi K. Perspectives for Highly-Sensitive PET--Based Medical Imaging Using $\beta+\gamma$ Coincidences. Acta Phys. Pol. 2015;127:1441-4.
37. Nelms AT, Graphs of the Compton Energy-Angle Relationship and the Klein-Nishina Formula from 10 KeV to 500 MeV. Phys. Today 1954;7:18.
38. Moskal P, Gajos A, Mohammed M, Chhokar J, Chug N, Curceanu C, et al. Testing CPT symmetry in ortho-positronium decays with positronium annihilation tomography. Nat. Commun 2021;12(1):5658.
39. Lång C, Habs D, Parodi K, Thirolf PG. Sub-millimeter nuclear medical imaging with high sensitivity in positron emission tomography using $\beta+\gamma$ coincidences. J. Instrum. 2014;9:P01008-8.
40. Martin CC, Christian BT, Satter MR, Nickerson LDH, Nickles RJ. Quantitative PET with positron emitters that emit prompt gamma rays. IEEE Trans Med Imaging 1995;14:681-7.